BEARINGLESS MOTOR WITH DSP CONTROL

Rafael R. Gomes[1], Richard M. Stephan[2], José Andrés Santisteban[3]
[1]UFRJ ramos@ufrj.br, [2] UFRJ rms@ufrj.br , [3]UFF jasantisteban@vm.uff.br

***Abstract* – The control of a bearingless motor using a Digital Signal Processor (DSP) is presented. The operation and a mathematical model are explained. An optimized performance is achieved using scheduled adaptive PD controllers, which parameters are function of the rotor speed. Finally, experimental results are shown.**

***Index Terms* – Electrical machines, magnetic bearings, scheduled adaptive control, DSP control.**

I. INTRODUCTION

The advantages of bearingless motors encourage researchers all over the world [1-3]. Beside space reduction, this technology allows the construction of frictionless motors, eliminating the need of lubrication and expanding the velocity operation limits. These characteristics open a wide range of applications in industrial, medical and aerospace fields.

Digital Signals Processors (DSP) are powerful tools in the control of bearingless motors. The DSP supports real-time control and on-line adjustments. This work presents the digital implementation of a scheduled adaptive control for a bearingless motor prototype. The model, operation and experimental results are explained.

II. THE BEARINGLESS PROTOTYPE

The bearingless motor is a device that provides both radial positioning and rotation of the rotor shaft, combining the functions of motor and radial bearing. A feedback control system makes this operation possible. The feedback control monitors the rotor position and produces electromagnetic restoring forces by currents imposed on each stator pole.

The system used in this work consists of two induction motors sharing the same shaft. Figure 1 shows a cut-view of the bearingless motor prototype. The dimensions are given in Fig. 2.

The bottom part may hold superconductors to act as axial bearing [4]. The prototype admits a maximum radial gap of 0.4*mm* between security bearings and the stator.

The displacement is measured with eddy-current sensors [5] disposed in two orthogonal directions as shown in Fig. 3. By difference of opposite sensors, voltage levels with linear variations of the radial displacement are obtained.

The rotor velocity is measured using an inductive proximity sensor [6] and a cylinder target with variable reluctance.

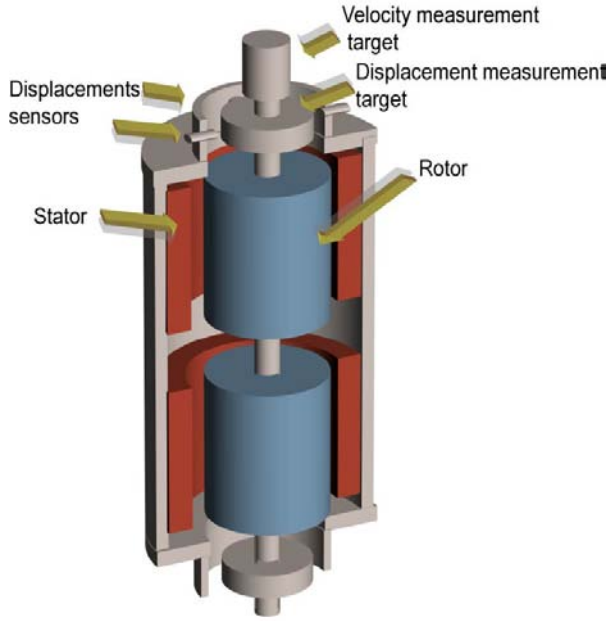

Fig. 1. Bearingless motor cut-view.

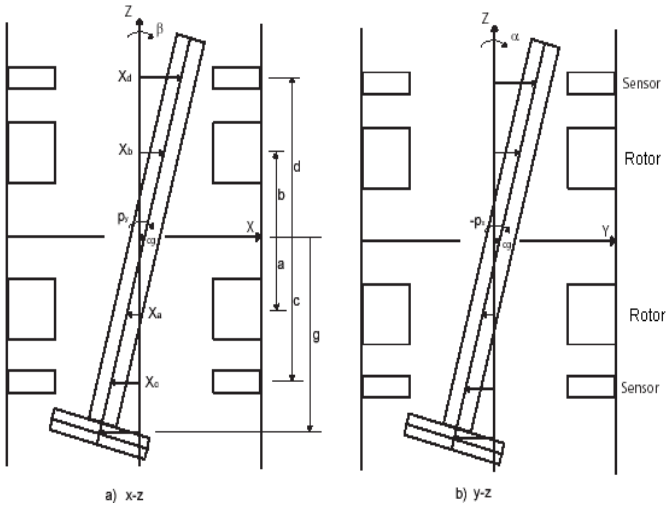

Fig. 2. Prototype mechanical dimensions.

$a = 68{,}0\times10^{-3}\,m$, $b = -82{,}8\times10^{-3}\,m$, $c = 148{,}0\times10^{-3}\,m$, $d = -163{,}0\times10^{-3}\,m$, $g = 218{,}0\times10^{-3}\,m$.

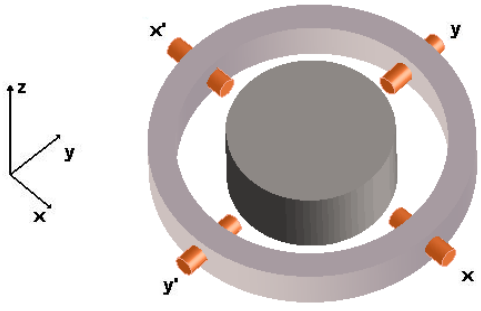

Fig.3. Position sensors

III. SYSTEM MODEL

A. Electromagnetic model

A two phases, four poles stator was used. In phase A, each pole winding can be independently controlled. In phase B, all poles are series connected. The positioning currents are imposed to phase A windings in a differential way. In equilibrium state, the rotor shaft is centralized and all currents applied to the four A phase poles have the same value. In this case, no radial force is produced.

According to the considerations presented in [7], the following procedure can be followed to determine the expression relating the electromagnetic force with differential electrical currents in phase A.

The linked flux relates with the currents by Eq. 1.

$$[\lambda] = [L(\lambda)][i]. \tag{1}$$

The electromagnetic force is given by Eq. 2.

$$F_e = \frac{1}{2}[i]^T \frac{d[L(h)]}{dh}[i]. \tag{2}$$

Using the transformations: $y_1 = y = h_0 + \Delta y$; $y_2 = (2h_0 - y) = h_0 - \Delta y$; $x_1 = x = h_0 + \Delta x$; $x_2 = (2h_0 - x) = h_0 - \Delta x$, where h_0 is the nominal air gap in the centered condition and considering small displacements, the following expression holds:

$$\frac{\partial[L(h)]}{\partial y_1} = -\frac{1}{2}N^2\mu\frac{A}{y^2}\begin{bmatrix} 1 & 0 & -\frac{1}{2} & -\frac{1}{2} \\ 0 & -1 & \frac{1}{2} & \frac{1}{2} \\ -\frac{1}{2} & \frac{1}{2} & 0 & 0 \\ -\frac{1}{2} & \frac{1}{2} & 0 & 0 \end{bmatrix}. \tag{3}$$

Supplying the stator windings with the following currents:

$$i_{y1} = (i_0 + \Delta i_y)\cos\omega t, \tag{4}$$

$$i_{y2} = (i_0 - \Delta i_y)\cos\omega t, \tag{5}$$

$$i_{x1} = (i_0 + \Delta i_x)\cos\omega t, \tag{6}$$

$$i_{x2} = (i_0 - \Delta i_x)\cos\omega t, \tag{7}$$

the electromagnetic force is given by Eq. 8.

$$F_y = F_1 - F_2 = -2N^2\mu\frac{A}{y^2}[i_0\Delta i_y]\cos^2\omega t \tag{8}$$

B. Mechanical model

As the main objective of this work was to evaluate the DSP performance and the scheduled adaptive controller, only the upper motor was used, the center of gravity acting as a pivot. Thus, the model presented in Fig. 2 is simplified as shown in Fig. 4.

Since the rotor is considered to be pivoted, only the magnetic bearing forces acting at an axial distance "*b*" from the pivot point "O" contribute to the mechanical positioning of the rotor.

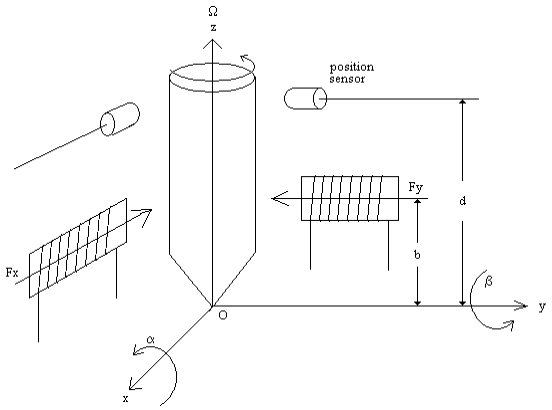

Fig. 4. Electromechanical model.

From a control point of view, it is convenient to express the mechanical model in terms of the radial displacement coordinates "*x*" and "*y*" provided by the displacement sensors positioned at an axial distance "d" from the pivot point "O". Assuming that the angular displacements $\alpha = -y/d$ and $\beta = x/d$ are small, the following relation can be written:

$$\begin{bmatrix} I_0 & 0 \\ 0 & I_9 \end{bmatrix}\begin{Bmatrix} \ddot{y} \\ \ddot{x} \end{Bmatrix} + \begin{bmatrix} 0 & -I_p\Omega \\ I_p\Omega & 0 \end{bmatrix}\begin{Bmatrix} \dot{y} \\ \dot{x} \end{Bmatrix} = \begin{Bmatrix} bdF_y \\ bdF_x \end{Bmatrix} \tag{9}$$

This matrix equation can be given as a system of two differential equations:

$$\ddot{x} = \frac{I_p}{I_0}\Omega\dot{y} + \frac{bd}{I_0}F_x, \tag{10}$$

$$\ddot{y} = -\frac{I_p}{I_0}\Omega\dot{x} + \frac{bd}{I_0}F_y. \tag{11}$$

These equations lead the block diagram shown in Fig. 5.

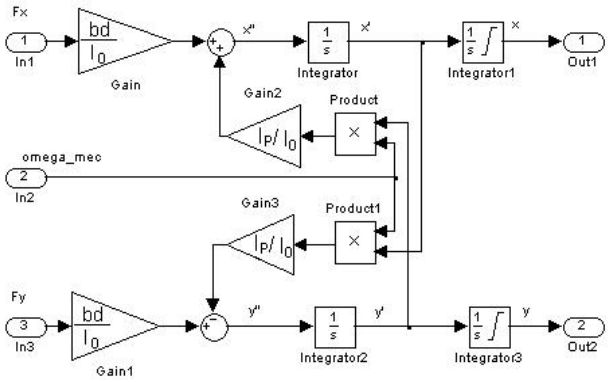

Fig. 5. Block diagram of the mechanical model.

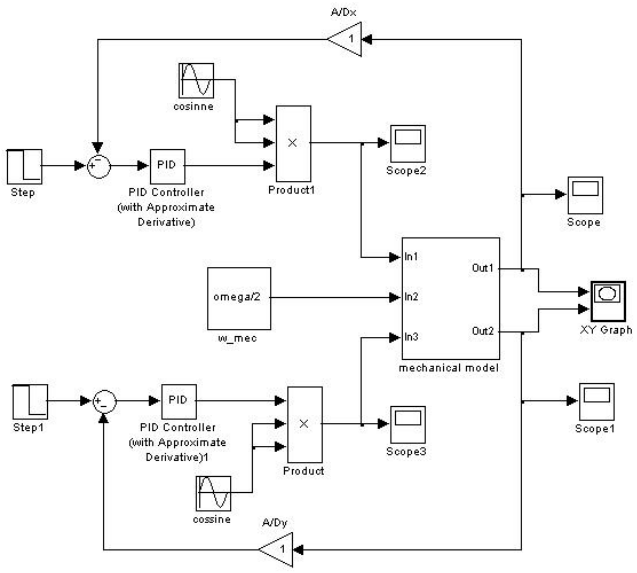

Fig. 6. Block diagram of the control system.

IV. THE CONTROL SYSTEM

A. Position Control System

According to the mechanical and electromagnetic models presented in the previous sections, the simulation model shown in Fig. 6 is obtained. The moments of inertia I_0 and I_p of the prototype were measured and found to be: I_0= 50.3x10^{-3} kg.m^2, I_p=2.17x10^{-3} kg.m^2, while the heights "*b*" and "*d*" are: *b*= 0.0828 m, *d*= 0.163 m.

A simple PD controller may be used to stabilize the rotor position for each control axis [8]. However, keeping the PD controller parameters unchanged cause degradation of performance, principally at high speeds. This is due to the gyroscopic effect as shown in Figure 7, where the system behavior for three speeds, assuming fixed and adaptive PD controller parameters, is simulated.

It can be seen that the gyroscopic effect in higher velocities is larger than at lower ones. The PD parameters are adjusted to give an optimized performance in function of the rotor speed to minimize the gyroscopic effect [9]. The optimized parameters are stored in a look-up table.

B. Speed Control System

An independent PI controller was used for the speed control. The speed is measured by inductive proximity sensors as already explained. The control system is based on a slip control with anti-windup PI controller and slip limits.

C. Complete Control System

The complete control system is depicted in Fig.8.

V. THE DSP SYSTEM

The control algorithm was developed in a fixed point digital signal processor (F2812 from Texas Instruments), which was programmed using C language.

The current signals are acquired by Hall effect sensors. These signals are conditioned to A/D voltage levels. The digital outputs are used to send the trigger signals for each of the IGBT bridges connected to the stator windings. The signals cos(ωt) and sin(ωt) are internally created using look-up tables.

The position control in each orthogonal direction is given by PD controllers, which parameters are function of the rotor speed. The current control was implemented in the same algorithm.

A. Initialization Procedure

The initialization procedure consists on setting internal DSP flags and vectors initialization. This procedure can be seen in Fig.9. The initialization algorithm performs data acquisitions to determine the offset of the input values.

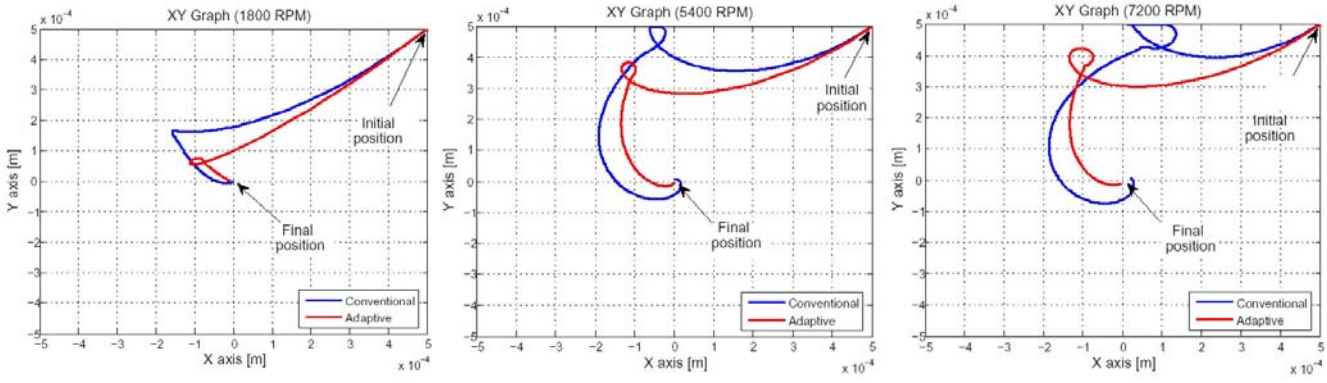

(a) (b) (c)

Figure 7. Simulated transient responses for conventional (Blue) and adaptive (Red) controller.
a) 1800 rpm, b) 5400 rpm, c) 7200 rpm.

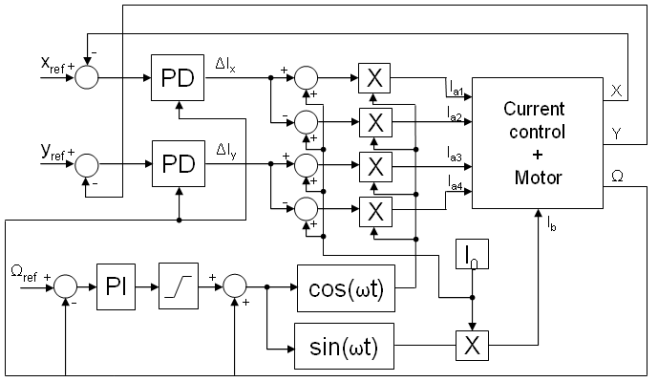

Figure 8. Control system implementation model.

B. System Control Algorithm

The system control algorithm performs the overall system control based on DSP interruptions. The block diagram representing the algorithm control logic is shown in Fig. 10. The instantaneous values of phase currents (4 phases A currents and 1 phase B current), rotor positions (x and y) and rotor speed are treated by motion filters. The function of a motion filter is to suppress measuring noise and spurious signals. After that, the values of all currents are compensated by the offset values determined in the initialization procedure. Beyond this point, the control system algorithm has two branches: one for the position and the other for the speed control. The position control branch adjusts the PID parameters if the adaptive control is selected. This PID parameter adjustment is realized using a look-up table representing the optimum PID parameters as a function of the rotor speed. The optimized values are determined by off-line mathematic simulations [9]. The speed control branch limits the maximum slip.

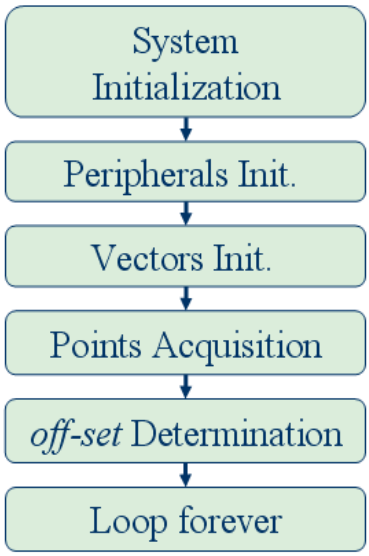

Figure 9. Initialization procedure.

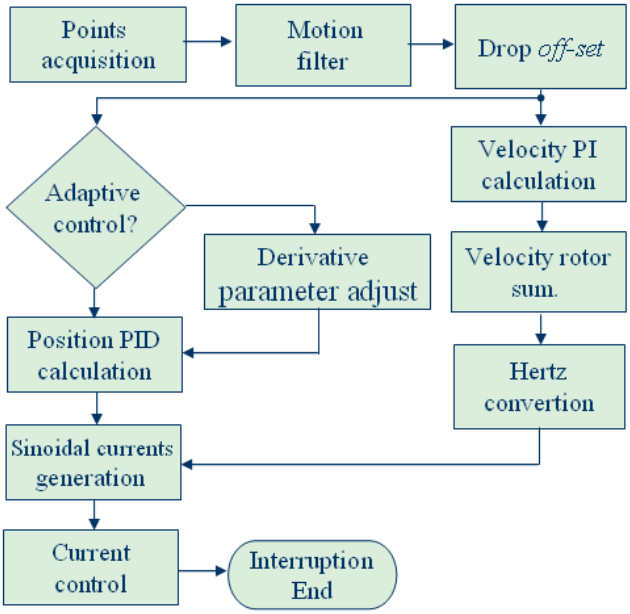

Figure 10. System control algorithm.

The output of the position and speed controllers are used to generate the sinusoidal currents references. The position PID controller modulates the imposed current amplitude and the speed PI dictates the frequency.

The current control is done by hysteresis current controllers (bang-bang), which compare the instantaneous motor currents with the reference values determined by the algorithm.

VI. EXPERIMENTAL RESULTS

Figure 11 shows the maximal orbit circumference and the rotor position in a XY oscilloscope image for a speed of 2000 RPM without adaptive control. The time response for a step change of 0,1µm in the Y reference is shown in Fig.12. It can be seen that there is a slight coupling between the X and Y axes. These results can be improved with the scheduled adaptive control as shown in Fig. 13 and Fig. 14. Figure 15 shows the system behavior for a motor start up with final speed of 2000 RPM.

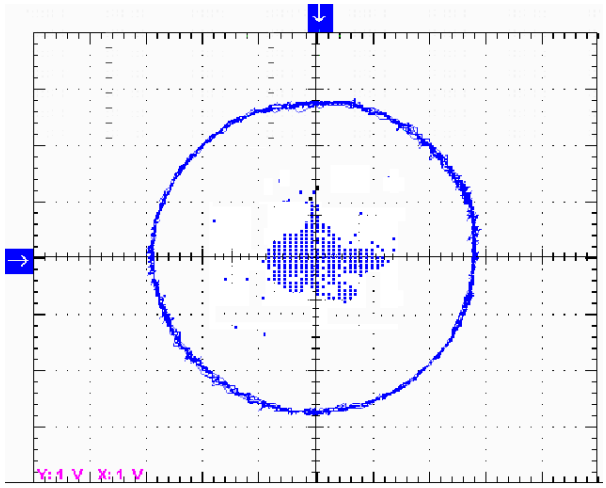

Fig. 11. Maximal orbit circumference and rotor position without scheduled adaptive control.

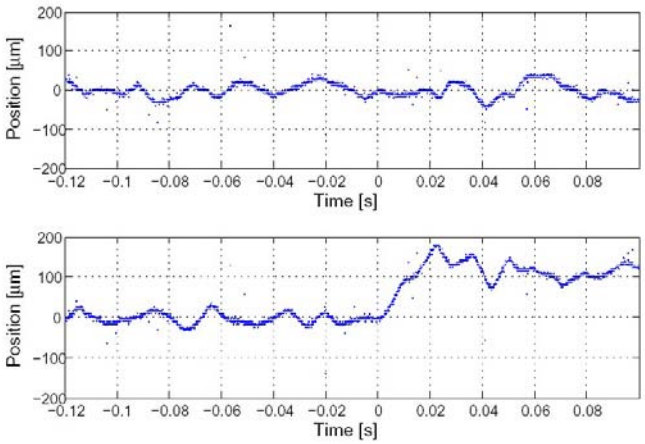

Fig. 12. Time response for a step change of 0,1µm in the Y reference at 2000 RPM without adaptive control.

VII. CONCLUSION

This work presented the control of a bearingless motor using a DSP platform. This platform offers a reliable and flexible kind of implementation. Optimized scheduled adaptive controllers improve the dynamic behavior of the system. The scheduled adaptive control changes the parameters of the PID position controllers to offer a good performance to different speeds. The parameters of the scheduled adaptive control are obtained through mathematic simulations using the well-determined system model. The control system algorithm was presented. Experimental results show the effectiveness of the scheduled control system.

ACKNOWLEDGEMENT

The authors would like to thank CNPq and CAPES for financial support and Mr. Wilmar Kauss for the technical collaboration.

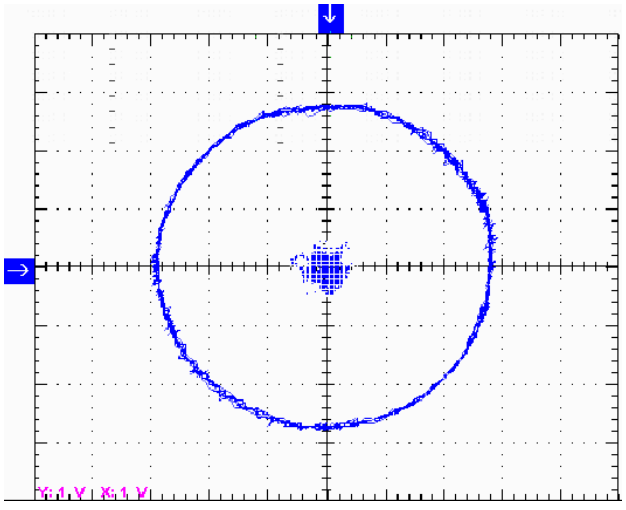

Fig. 13. Maximal orbit circumference and rotor position with scheduled adaptive control.

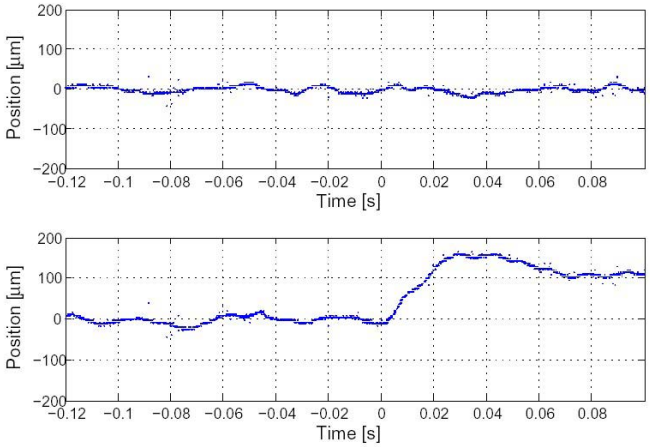

Fig. 14. Step response for a step change of 0,1µm in the Y reference at 2000 RPM with scheduled adaptive control.

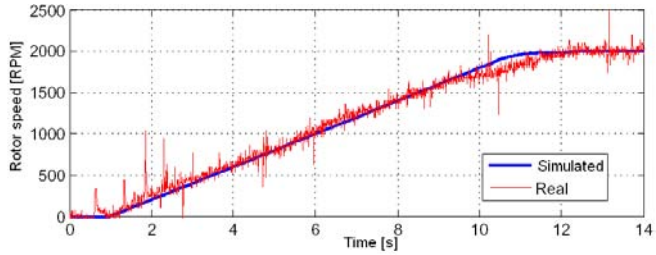

Fig. 15. Motor start up with final speed of 2000 RPM.

REFERENCES

[1] Chiba, A.; Deido, T.; Fukao, T.; Rahman, M.A.; **"**An analysis of bearingless AC motors"**,** *IEEE Transactions on Energy Conversion*, Volume 9, Issue 1, March, 1994, Page(s):61 – 68.

[2] He Yikang; Nian Heng; "Analytical model and feedback control of the levitation force for an induction-type bearingless motor", *The Fifth International Conference on Power Electronics and Drive Systems*, Volume 1, November, 2003, Page(s):242 – 246.

[3] Amirulddin, U.A.U.; Asher, G.M.; Sewell, P.; Bradley, K.J.; "Dynamic field modelling of torque and radial forces in vector-controlled induction machines with bearing relief", *IEE Proceedings on Electric Power Applications*, Volume 152, Issue 4, July 2005 Page(s):894 – 904.

[4] David, D., Del Nero Gomes A. C., Santisteban J. A., RIPPER, A., ANDRADE JR, R., NIKOLSKY, R. A. "Hybrid Levitating Rotor System with Radial Electromagnetic Motor-Bearings and Axial Superconducting Bearing", *The 16th International Conference on Magnetically Levitated Systems and Linear Drives MAGLEV'2000*, 2000, Rio de Janeiro. Proceeedings of the MAGLEV'2000. , 2000. p.441–446.

[5] User's manual, model 1195-510, Shinkawa Electric Co, Tokyo, Japan.

[6] User´s manual, DD 2003 (monitor), IZ5052 (sensor), IFM electronics.

[7] J. A. Santisteban, "Estudo da influência da carga torcional sobre o posicionamento radial de um motor-mancal", D.Sc. Thesis, COPPE/UFRJ, Rio de Janeiro, Brazil, March, 1999.
[8] J. A. Santisteban, R.M Stephan, "Analysis and Control of a Loaded Bearingless Machine", *IEEE International Magnetic Conference*, Kyongju, Korea, May, 1999, pp.146-148.
[9] R. R. Gomes, J. A. Santisteban, R. M. Stephan, "Optimized Performance of a Motor-Bearing", *ABCM Symposium Series in Mechatronics, Vol.2, Section VI, pp. 417-424 (http:/www.abcm.org.br/symposiumSeries/).*